HHS Public Access

Author manuscript

AJNR Am J Neuroradiol. Author manuscript; available in PMC 2016 July 01.

Published in final edited form as:

AJNR Am J Neuroradiol. 2016 January ; 37(1): 80–87. doi:10.3174/ajnr.A4478.

On the Use of DSC-MRI for Measuring Vascular Permeability

Jack T Skinner[1,2], **Paul L Moots**[3], **Gregory D Ayers**[4], and **C. Chad Quarles**[1,2,5,6]

[1]Vanderbilt University Institute of Imaging Science, Vanderbilt University

[2]Department of Radiology and Radiological Sciences, Vanderbilt University School of Medicine

[3]Department of Neurology, Vanderbilt University School of Medicine

[4]Department of Biostatistics, Vanderbilt University School of Medicine

[5]Department of Cancer Biology, Vanderbilt University

[6]Department of Biomedical Engineering, Vanderbilt University

Abstract

Background and Purpose—Contrast agent (CA) extravasation has been shown to confound brain tumor perfusion measurements using DSC-MRI, necessitating the use of correction techniques (e.g. Weisskoff, Bjornerud). Model parameters (K_2 and K_a) postulated to reflect vessel permeability can be extracted from these correction methods, however the biophysical interpretation of these parameters and their relationship to commonly used MR measures of vascular permeability (e.g. K^{trans}) remains unclear. Given that vascular density, as assessed by blood volume, and vascular permeability, as reflected by K^{trans} (and potentially K_2 or K_a), report on unique and clinically informative vascular characteristics, there is a compelling interest to simultaneously assess these features.

Materials and Methods—Multi-echo DSC-MRI data was acquired, allowing the simultaneous computation and voxel-wise comparison of single- and dual-echo derived measures of K_2, K_a and K^{trans} in glioma patients. This acquisition enabled the investigation of competing T_1 and T_2^* leakage effects and echo time dependency on these parameters.

Results—K_2 and K_a displayed non-significant ($p = 0.150$ and $p = 0.060$, respectively) voxel-wise linear correlations with K^{trans}, while a significant ($p < 0.0001$) inverse relationship was observed between K_2 and K_a [$r^2 = 0.466–0.984$]. Significantly different ($p < 0.005$) mean estimates were found between voxels exhibiting predominately T_1 or T_2^* leakage effects for K_2 and K_a. K^{trans}, however, was observed to be similar between these voxels (0.109 min^{-1} vs 0.092 min^{-1}). Significant differences ($p < 0.0005$) in v_e (0.285 vs 0.167) were also observed between cohorts. Additionally, K_2 and K_a were found to have a significant quadratic relationship ($p = 0.031$ and $p = 0.005$, respectively) with v_e.

Conclusion—Estimates of vascular permeability in brain tumors may be simultaneously acquired from multiple-echo DSC-MRI via K^{trans}, however caution should be used in assuming a similar relationship for K_2 and K_a.

Please send correspondence to: C. Chad Quarles, Vanderbilt University Institute of Imaging Science, AA 1105 Medical Center North, 1161 21st Avenue South, Nashville, TN 37232-2310, USA, Phone: (615) 322-6215, chad.quarles@vanderbilt.edu.

Keywords

permeability; perfusion; leakage; DSC-MRI; dynamic contrast enhanced; multi-echo; tumor

Introduction

Brain tumors are characterized by abnormal, poorly constructed vasculature that is often permeable[1], making them identifiable on contrast-enhanced MR images. With dynamic contrast enhanced (DCE)-MRI methods, contrast agent (CA) wash-in and extravasation alters the tissue T_1 relaxation time and kinetic analysis of the associated signal change permits the computation of the volume transfer constant, K^{trans}, which reflects vascular permeability and perfusion. In dynamic susceptibility contrast (DSC)-MRI studies, CA flowing through blood vessels decreases tissue T_2^* and the acquired signal changes can be used to estimate tumor blood volume. However, CA extravasation has been shown to confound measurements of tissue perfusion (e.g. underestimation of blood volume), particularly in high-grade brain tumors[2–4]. When corrected for CA leakage effects, DSC-MRI measures of blood volume correlate with brain tumor grade and may be useful for monitoring treatment response[2, 5].

CA extravasation leads to simultaneous and competing T_1 and T_2^* effects that can substantially alter the temporal dynamics of DSC-MRI signals[2, 6], necessitating the use of correction techniques. One such technique, developed by Weisskoff *et al*.[7] and Boxerman *et al*.[2], incorporates knowledge of the average signal time-course across the brain in non-enhancing voxels to model and correct time-courses in tumor voxels. As a result, a parameter termed 'K_2' can be extracted that reflects the degree of CA extravasation. Though initially developed to correct T_1 leakage effects, the Weisskoff method has been adapted to also account for T_2^* leakage effects[8]. A known limitation of this method, however, is that it assumes the mean transit times (MTT) of both healthy and diseased tissue to be equal, which has been observed to not be true in gliomas[9]. To address this issue, Bjornerud *et al.* recently developed a MTT insensitive approach for correcting both T_1 and T_2^* leakage effects on DSC-MRI signals[10, 11]. In this method, the tissue residue function, which describes the CA passage through a voxel, is separated into an intravascular and an extravascular component, from which a parameter 'K_a' (similar to K_2) can be estimated. A third technique aims to remove T_1-based CA leakage effects, through the use of multiple gradient-echo acquisitions[3, 12–14]. A feature of this approach is that dynamic T_1-weighted information can be separated and quantified[15–17]. Traditional pharmacokinetic modeling[18, 19] can then be applied to this data to extract a measure of K^{trans}, in a manner similar to DCE-MRI. This approach has been validated in animal brain tumor models and has been recently applied in high-grade glioma patients[16, 17, 20]. To collect both DCE-MRI and DSC-MRI datasets, an alternative strategy is to acquire traditional DCE-MRI data during a pre-load injection of contrast agent, which is a technique also commonly used to reduce T_1 leakage effects in single-echo based DSC-MRI data[3].

In the case of brain tumors, K^{trans} is largely considered to reflect vascular permeability[19] and has demonstrated promise in tumor grading[21, 22] and identifying disease progression and

treatment response[23–26]. It has been postulated that measures of K_2 and K_a may also directly report on vascular permeability, however their relationship with imaging biomarkers such as K^{trans} is not entirely clear and may be dependent on CA kinetics, tissue microstructure, and imaging parameters. Preliminary studies have also investigated the use of K_2 and K_a for assessing tumor type[27], grade[28, 29], and treatment response[11].

Inherent to the aforementioned DSC-MRI correction techniques, estimates of K_2 and K_a may assume positive or negative values depending on whether T_1 ($+K_2$, $-K_a$) or T_2^* ($-K_2$, $+K_a$) leakage effects are the dominating source of signal error. Unlike K_2 and K_a, estimates of K^{trans} assume the use of a 'purely' T_1-weighted signal and, therefore, presume insensitivity to competing T_1 and T_2^* leakage effects. In this regard, a previous simulation study reported a non-linear relationship between K_a and K^{trans} when large flip angles (>70) were used[10]. In a follow up *in vivo* study[11], a positive quadratic relationship between K_a and K^{trans} was observed. A more recent study found a positive linear correlation between K_2 and K^{trans} when comparing maximum whole tumor values across patients[30]. These studies, however, were limited to ROI-based estimates and measures of K^{trans} acquired from separate DCE-MRI acquisitions, and did not take into consideration the dominating CA leakage effect.

As suggested by previous works, the presence of simultaneous T_1 and T_2^* leakage effects within a tumor may influence the magnitude and interpretation of K_2 and K_a. The overarching goal of this study, therefore, was to investigate the contribution of both T_1 and T_2^* effects on K_2 and K_a, while evaluating these parameters as imaging biomarkers of vascular permeability in brain tumors. This was achieved through voxel-wise comparisons of DSC-MRI derived measures of K_2, K_a, and K^{trans} using the previously described methods. The multi-echo nature of this study allowed simultaneous measurement of these parameters from the same data set, permitting a more accurate comparison free of registration errors and/or sequence specific differences. In addition, the multi-echo data allowed further exploration of potential echo time dependencies of both Weisskoff and Bjornerud correction techniques.

Methods

MRI data were acquired in high-grade glioma patients (n = 7, See Table 1) under Vanderbilt University Institutional Review Board guidelines at 3T (Achieva, Philips Healthcare, Best, The Netherlands) using a 32-channel head coil. Multiple flip angle (MFA) data (TR = 7.6ms, TE = 4.6ms, FA = 2°-20° in 2° increments) were acquired to compute pre-contrast R_1 (R_{10}) maps. Dual-echo (DE) DSC-MRI data were then acquired using either a dual gradient-echo (DGE) EPI or SAGE EPI protocol[17, 31] with: TR = 1.5s (DGE) or 1.8s (SAGE), TE_1/TE_2 = 7.0/31.0ms (DGE) or 8.3/25ms (SAGE), SENSE = 2, FOV = 240 × 240mm^2, Reconstructed Voxel Size = 2.5 × 2.5 × 5.0mm^3, and slices = 15. For SAGE data, only the first two echoes were used in the analysis. Measurements were made before, during, and after administration of Gd-DTPA (0.1 mmol/kg, 4ml/s infusion rate followed by a 20ml saline flush). The scan duration was 7.5 minutes, including 80s of pre-bolus baseline data. A high-resolution T_1-weighted data set was collected following the DSC-MRI experiment.

Dynamic estimates of ΔR_2^* were computed for each echo ($\Delta R^*_{2,TE1}$ and $\Delta R^*_{2,TE2}$) and for the dual-echo data ($\Delta R^*_{2,DE}$) as previously described[12, 13].

K_2 Computation

The method proposed by Weisskoff *et al.*[7] allows the extraction of K_2 from Eq 1,

$$\Delta\tilde{R}_2^*(t) \approx K_1 \cdot \overline{\Delta R_2^*(t)} - K_2 \int_0^t \overline{\Delta R_2^*(t')} dt' \quad (1)$$

where $\overline{\Delta R_2^*}$ is the average ΔR_2^* from a mask of non-enhancing brain voxels and $\Delta\tilde{R}_2^*$ is the leakage affected estimate of ΔR_2^*. A voxel-wise least squares fit to Eq. 1 was performed to extract K_2 using 80s of pre-bolus baseline data and 70s of post-bolus data (2.5 min total) consistent with previous reports[2, 3, 29].

K_a Computation

In the presence of CA extravasation, the tissue concentration time-course, $C_t(t)$, can be represented as

$$C_t(t) = f \int_0^t R(t) \cdot C_p(t-\tau) d\tau + K_a \int_{T_c}^{t'} C_p(t'-\tau) \cdot \exp(-K_a(\tau - T_c)/\nu_e) d\tau \quad (2)$$

where f is proportional to tissue blood flow, $R(t)$ is defined as the tissue-specific residue function, T_c is the capillary transit time of the CA, v_e is the extracellular-extravascular volume fraction, and C_p is the tracer [CA] in plasma (computed from an AIF extracted from the dual-echo data using an automated selection process[32, 33]). In DSC-MRI, $C_t(t)$ is estimated in relative terms through measurements of $\Delta R_{2,t}^*(t)$[10], where $\Delta R_{2,t}^*(t) \propto r_2^* \cdot C_t(t)$ and r_2^* is the effective transverse relaxivity. Circular deconvolution of Eq. 2 with the AIF[34] (over the same time-course used in the Weisskoff correction), results in a composite residue function $H(t)$ described by an early vascular phase ($0 \le t < T_c$) and an extravasation phase ($t \ge T_c$)[10]:

$$H(t) \approx f \cdot R(t) \quad 0 \le t < T_c \quad (3)$$

$$H(t) \approx K_a \cdot \exp(-K_a(t - T_c)/\nu_e) \quad t \ge T_c$$

In the context of a single-echo DSC-MRI acquisition, $H(t) \approx K_a$ for $t >> T_c$. In this study, K_a was estimated as the mean value of $H(t)$ following a time T_c, equivalent to 1.5× the mean transit time (*MTT*), up to $H(t=60s)$.

K^{trans} Computation

To compute an estimate of K^{trans} from multi-echo DSC-MRI data, a T_1-weighted signal time-course ($S_{T1w}(t)$) was first extracted from dual-echo data via Eq. 4[15, 16, 35].

$$S_{T1w}(t) = S_{TE_1}(t) \cdot e^{ln\left(\frac{S_{TE_1}(t)}{S_{TE_2}(t)}\right)\cdot\left(\frac{TE_1}{TE_2 - TE_1}\right)} \quad (4)$$

A pre-contrast R_1 (R_{10}) map was combined with the $S_{T1w}(t)$ data to produce dynamic R_1 time-courses ($R_{1t}(t)$) for each voxel[36, 37]. K^{trans} and v_e were estimated by fitting $R_{1t}(t)$ and $C_p(t)$ (AIF) with the standard Tofts model[18, 19].

Voxel Selection

Voxels selected for this analysis were obtained from enhancing regions on the post-Gd T_1-weighted images, determined using a 50% signal threshold (based on the maximum signal intensity in tumor-containing slices) over a manually drawn tumor ROI. These voxels were further categorized by the predominate leakage effect (T_1 or T_2^*) exhibited in their dynamic ΔR_2^* time-course. In this study, 'T_2^* voxels' were defined by a positive mean ΔR_2^* over the last 20s of the time-course used for computation of K_a and K_2. 'T_1 voxels' were defined as those in which this estimate was negative.

Statistical Analysis

Voxel-wise measures of K_2 and K_a were compared with K^{trans} and v_e to examine the relationship between these parameters. Associations between the aforementioned parameters were first analyzed on an individual basis using simple linear regression and reported using the r-squared (r^2) statistic. Unless otherwise noted, group voxel-wise comparisons were conducted using analysis of covariance in a generalized linear model for repeated measures. Generalized estimating equations (GEE) were used with an exchangeable covariance structure to model the correlation among voxels across patients.

Results

Fig. 1a shows a representative uncorrected tumor ΔR_2^* time-courses for each echo time and the dual-echo signal, along with the associated Weisskoff model fit. Fig. 1b shows the corresponding tissue residue functions used to compute K_a from the same patient. The computed K^{trans}, K_2, and K_a maps (overlaid on post-Gd T_1-weighted images) for this patient (at TE_2) can be seen in Fig. 2b–d, respectively, along with the corresponding post-Gd T_1-weighted image (Fig. 2a). Fig. 3a and 3b show an example voxel-wise comparison of K_2 and K_a (computed at TE_2) with the parameter K^{trans}. The range of correlations at TE_2 were r^2 = [0.014 – 0.430] for K_2 and r^2 = [0.0001 – 0.403] for K_a. Across patients, both K_2 and K_a were found to have non-significant ($p = 0.150$ and $p = 0.060$, respectively) linear correlations with K^{trans}. A significant ($p < 0.0001$) inverse relationship was observed (Fig. 3c), however, between K_2 and K_a [r^2 = 0.466–0.984]. To help elucidate these observed relationships, further analysis was performed.

With the availability of multi-echo data, the effect of echo time on K_2 and K_a was investigated. Fig. 4a and 4b show box plots using the median values of K_2 and K_a, across all patients. A statistically significant difference (Mann-Whitney U test) was observed between K_2 at TE_1 and TE_2 ($p<0.001$), K_2 at TE_1 and DE ($p<0.001$), and K_2 at TE_2 and DE ($p<0.01$) acquisitions. Similar differences were observed for K_a. For TE_2, voxel-wise estimates of K_2

were observed to be predominately positive for high-grade gliomas whereas K_a was predominately negative. A decrease in echo time (TE_1) resulted in a broader voxel-wise distribution of values across patients with estimates of K_2 becoming increasingly positive and K_a becoming increasingly negative. The computation of K_2 using the $\Delta R^*_{2,DE}$ time-course resulted in a negative shift in the distribution of values, with an increase in the number of voxels near $K_2 = 0$. A similar shift in the distribution towards positive values was observed for K_a.

Fig. 5 shows the contribution of both T_1 and T_2^* leakage effects on the relaxation rate time-courses. Fig. 5a shows the mean ΔR_2^* time course (TE_2) for a tumor ROI from patient 2. The resulting ΔR_1 time-course from the same tumor can be seen in Fig. 5b. Though the ΔR_2^* time-course appears to show no appreciable signs of CA leakage, the ΔR_1 time-course exhibits large changes in R_1 with bolus passage. This indicates CA extravasation and results in a moderate estimate of K^{trans}. Similarly, focusing on the smallest 10% of all voxels (based on the magnitude of K_a) in a given patient, $K_a = -0.043 \pm 0.050$ min^{-1}, $K_2 = 0.113 \pm 0.553$ min^{-1}, and $K^{trans} = 0.060 \pm 0.099$ min^{-1} (weighted mean ($mean_w$) ± pooled std (std_p)). Fig. 5c and 5d show mean ΔR_2^* and ΔR_1 time-courses from the same tumor with voxels separated by predominate T_1 or T_2^* leakage effects. Note that, in Fig. 5c and 5d, voxels from the same tumor exhibited positive and negative values of K_2 and K_a, while K^{trans} was observed to be almost identical between the two cohorts.

Table 2 displays the mean estimates of K_2, K_a, and K^{trans} (separated by T_1 and T_2^* voxels) across all patients. On average, 63% of voxels in the high-grade gliomas were found to predominately exhibit T_1 leakage effects. In addition, a significant difference ($p < 0.005$, paired t-test) was observed, across patients, between mean estimates from T_1 and T_2^* voxel cohorts for both K_2 and K_a. While the difference between T_1 and T_2^* cohorts for K^{trans} trended toward significance ($p \approx 0.05$), the weighted mean for each cohort across patients were similar (0.109 min^{-1} vs 0.092 min^{-1}). In all voxels across patients, we observed $v_e = 0.241 \pm 0.207$. When separated by leakage effect, a significant difference ($p < 0.0005$, paired t-test) in mean estimates of v_e was also observed. Additionally, both K_2 and K_a were found to have a significant quadratic relationship ($p = 0.031$ and $p = 0.005$, respectively) with v_e.

Discussion

DCE-MRI estimates of vascular permeability, often reported via K^{trans}, have been shown to be helpful in deciphering brain tumor grade[21] and in predicting disease prognosis[25, 38]. Unlike DCE-MRI, DSC-MRI acquisitions can actually be confounded by the increased vascular permeability present in brain tumors, requiring strategies for leakage correction of the MR signal time-courses. Rate constants (K_2 and K_a) computed from these correction techniques have been suggested to reflect vessel permeability[7, 28]. To evaluate this relationship, a simultaneous comparison between K^{trans} and the parameters K_2 and K_a was performed using multi-echo DSC-MRI. In general, the range of K_2 and K_a estimates in this study were observed to be larger than that of K^{trans}, though they were consistent with previous measures in brain tumors[8, 10, 28]. Voxel-wise linear relationships between K_2 and K_a and the parameter K^{trans} were found to be non-significant when computed from the same data set. Though a non-linear relationship between K_a and K^{trans} was previously presented

in simulations[10], this work provides additional *in vivo* confirmation. The individual correlations observed here between K_2 and K^{trans} in gliomas were similar to that observed by Bonekamp *et al*. using max K^{trans} and K_2 values from whole tumor ROIs[30]. Though the lack of a strong linear correlation with K^{trans} suggests potential limitations with extracting permeability estimates from DSC-MRI correction methods themselves, it should not, however, be interpreted as a failure of these techniques to reliably correct CBV measures for CA leakage.

The effect of echo time on K_2 and K_a was also studied. From Fig. 4 we observed a significant increase (decrease) in estimates of K_2 (K_a) with a shorter echo time. This is due, in part, to the decrease in T_2^* weighting with decreasing echo time and subsequent dominance of T_1 leakage effects. Liu et al. previously explored the effect of echo time on K_2 in numerical simulations[8] and noted that changes in the actual vascular permeability should not affect the polarity of K_2, though changes in imaging parameters (e.g. echo time) could. Prior to the current study, a similar analysis with K_a had not yet been performed.

In addition to echo time, the intrinsic presence of competing and simultaneous T_1 and T_2^* leakage effects, within a given voxel, were integral in determining the value of K_2 and K_a. As shown in Fig. 5, competing T_1 and T_2^* leakage effects can produce a ΔR_2^* time-course that paradoxically appears to be free of CA extravasation effects. This is misleading, as the dynamic ΔR_1 information reveals appreciable CA leakage, resulting in moderate estimates of K^{trans}. As noted by Bjornerud *et al*., the presence of both T_1 and T_2^* relaxation effects in the extracellular-extravascular space may drive K_a (and K_2) towards 0, resulting in artifactually low estimates. As an example, in the smallest 10% of all voxels (based on the magnitude of K_a), the mean K^{trans} was observed to be 50% larger than $|K_a|$. Conversely, the magnitude of the mean K_a was ≈3× larger than K^{trans} when computed using all voxels. Additionally, the mean value of K_2 and K_a, computed from the aforementioned subset of voxels (smallest 10%), were almost an order of magnitude smaller than the respective mean K_2 and K_a computed using all voxels. These findings clearly have implications on the reliability of these parameters as measures of vascular permeability.

In general, the relationship of K_2 and K_a with K^{trans} may indicate an inaccurate assumption that these parameters solely reflect vessel permeability in brain tumors. When separated into T_1 and T_2^* voxel cohorts, the mean values of K_2 and K_a across patients were found to be significantly different from one another (Table 2). The same was true for v_e. Similar to the previous observation between K_a and K^{trans} *in vivo*[11], a significant quadratic relationship was observed between K_2 and K_a and v_e across all patients. To this end, a recent theoretical study by Liu *et al*. demonstrated a potential relationship between v_e and the ratio of the parameters K_1 and K_2 from the Weisskoff correction method[39]. These results indicate that K_2 and K_a may also be influenced by the extravasation space of the CA.

The data in Table 2 also revealed that 'T_1 voxels' demonstrated larger v_e values than those found in 'T_2^* voxels'. This likely originates from the underlying biophysical basis of T_1 and T_2^* leakage effects. As in DCE-MRI, T_1 leakage effects result from the direct interaction of CA with the extracellular-extravascular water. Accordingly, the physiological factors that drive the tissue [CA] (compartmental volume fractions, perfusion and vascular permeability)

as well as physical properties (CA T_1 relaxivity, pre-contrast T_1) and pulse sequence parameters (TR, flip angle) all influence the shape and magnitude of T_1 leakage effects on DSC-MRI signals. In addition to physiological factors and imaging parameters, T_2^* leakage effects are influenced by intravoxel susceptibility differences created by the spatial distribution of the CA within a voxel. Recently, Semmineh *et al*. demonstrated that these effects are predominantly influenced by cellular properties including density, size, distribution and shape[40]. Consistent with the results presented herein, stronger T_2^* leakage effects were observed for tissues with higher cell density (or lower v_e). In general, the dependency of T_2^* leakage effects on tumor cellularity manifests as changes in the CA's effective T_2^* relaxivity. So unlike T_1 leakage effects, where the CA's T_1 relaxivity is essentially constant within and across tumors, the T_2^* relaxivity may vary from voxel to voxel as the cellular properties change[41].

The variable CA T_2^* relaxivity also has important implications on the interpretation of the extracted K_2 and K_a parameters. Though voxels were designated as predominantly exhibiting either T_1 or T_2^* leakage effects, each voxel's signal is the summation of these competing effects, as previously discussed. In the limiting case where T_2^* leakage effects are absent and the signals only reflect T_1 leakage effects, the K_2 and K_a parameters are primarily driven by the underlying CA kinetics and the assumptions built into the correction models and can be understood accordingly. However, when there are competing T_1 and T_2^* effects K_2 and K_a represent a complex balance between the CA kinetics and the tissue microstructure. Practically, this implies that a positive and negative estimate of K_2 or K_a of the same absolute value may not reflect the same combination of vascular permeability, tissue compartment size, or microstructural geometry. Similarly, K_2 and K_a values that are equivalent within or across tumors may not reflect the same underlying physiological environment since they could originate from unique combinations of competing T_1 and T_2^* effects. This observation may help further explain the discrepancies in using K_2 and K_a to evaluate tumor grade and to assess treatment response[11, 28, 29]. Computational studies that account for the underlying biophysical basis of the DSC-MRI signal could be used to systematically investigate and provide insight into the complex interaction between T_1 and T_2^* leakage effects and the derived K_2 and K_a values.

The use of multi-echo DSC-MRI in this study enabled measures of DCE-MRI signals and, subsequently, computation of the associated K^{trans} maps. As mentioned above, an alternative approach to collect both datasets in the same exam is to acquire DCE-MRI data during a pre-load of CA. This enables the use of traditional DCE-MRI pulse sequences, ones that typically have higher spatial (and lower temporal) resolution. For the purpose of the study, this approach would have enabled the comparison of more conventionally derived K^{trans} values to K_2 and K_a. It is interesting to note, however, that the addition of a pre-load to this study would have reduced T_1 leakage effects and increased T_2^* leakage effects. It is unclear how this would influence the correlation between K^{trans}, K_2 and K_a. Another limitation of this study is the small sample size. While the findings are likely to hold in a larger population of glioma patients, it would be valuable to expand the tumor types considered (e.g. primary central nervous system lymphoma and brain metastasis) since different

histologic subtypes have been shown to express varying degrees of T_1 and T_2^* leakage effects.

Conclusion

This study investigated the use of DSC-MRI for estimating vascular permeability in brain tumors. Implementation of common DSC-MRI leakage corrections techniques afforded the computation of rate constants (K_2 and K_a) postulated to report on vessel permeability. Additionally, the acquisition of multi-echo data allowed the computation of the DCE-MRI pharmacokinetic parameter K^{trans}. A voxel-wise comparison between the parameters K_2, K_a and K^{trans} revealed non-significant linear correlations that may be attributed, in part, to competing T_1 and T_2^* leakage effects and the effect of echo time on K_2 and K_a. Further investigation also revealed a significant quadratic relationship between K_2 and K_a and the DCE-MRI parameter v_e. Based on these findings, caution should be used in assuming a direct relationship between K_2 and K_a and vascular permeability in brain tumors. Furthermore, the acquisition of K^{trans} from multi-echo DSC-MRI data may provide a convenient method for simultaneously measuring vascular permeability and perfusion in brain tumors.

Acknowledgments

Grant Sponsors: NIH R01CA158079, NCI 2R25CA092043, VICC Young Ambassadors Grant (CCQ)

Abbreviations

CA	contrast agent
DSC	dynamic susceptibility contrast
DCE	dynamic contrast enhanced
K^{trans}	CA volume transfer constant
v_e	extracellular-extravascular volume fraction
CBV	cerebral blood volume
CBF	cerebral blood flow
MTT	mean transit time
MFA	multiple flip angle
AIF	arterial input function

References

1. Shubik P. Vascularization of tumors: a review. Journal of cancer research and clinical oncology. 1982; 103:211–226. [PubMed: 6181069]
2. Boxerman JL, Schmainda KM, Weisskoff RM. Relative cerebral blood volume maps corrected for contrast agent extravasation significantly correlate with glioma tumor grade, whereas uncorrected maps do not. AJNR Am J Neuroradiol. 2006; 27:859–867. [PubMed: 16611779]

3. Paulson ES, Schmainda KM. Comparison of dynamic susceptibility-weighted contrast-enhanced MR methods: recommendations for measuring relative cerebral blood volume in brain tumors. Radiology. 2008; 249:601–613. [PubMed: 18780827]
4. Quarles CC, Gochberg DF, Gore JC, et al. A theoretical framework to model DSC-MRI data acquired in the presence of contrast agent extravasation. Phys Med Biol. 2009; 54:5749–5766. [PubMed: 19729712]
5. Schmainda KM, Prah M, Connelly J, et al. Dynamic-susceptibility contrast agent MRI measures of relative cerebral blood volume predict response to bevacizumab in recurrent high-grade glioma. Neuro-oncology. 2014; 16:880–888. [PubMed: 24431219]
6. Paulson E, Prah DE, Schmainda KM. Compensation of Confounding T1 and T2 Dipolar and residual Susceptibility Effects in DSC-MRI using Dual-Echo SPIRAL. Proc Int Soc of Magn Reson Med. 2007:2811.
7. Weisskoff, RM.; Boxerman, JL.; Sorensen, AG. Proc Soc Magn Reson Med. San Francisco, California: 1994. Simultaneous blood volume and permeability mapping using a single Gd-based contrast agent; p. 279
8. Liu HL, Wu YY, Yang WS, et al. Is Weisskoff model valid for the correction of contrast agent extravasation with combined T1 and T2* effects in dynamic susceptibility contrast MRI? Med Phys. 2011; 38:802–809. [PubMed: 21452717]
9. Quarles CC, Ward BD, Schmainda KM. Improving the reliability of obtaining tumor hemodynamic parameters in the presence of contrast agent extravasation. Magn Reson Med. 2005; 53:1307–1316. [PubMed: 15906288]
10. Bjornerud A, Sorensen AG, Mouridsen K, et al. T1- and T2*-dominant extravasation correction in DSC-MRI: part I--theoretical considerations and implications for assessment of tumor hemodynamic properties. Journal of cerebral blood flow and metabolism : official journal of the International Society of Cerebral Blood Flow and Metabolism. 2011; 31:2041–2053.
11. Emblem KE, Bjornerud A, Mouridsen K, et al. T(1)- and T(2)(*)-dominant extravasation correction in DSC-MRI: part II-predicting patient outcome after a single dose of cediranib in recurrent glioblastoma patients. Journal of cerebral blood flow and metabolism : official journal of the International Society of Cerebral Blood Flow and Metabolism. 2011; 31:2054–2064.
12. Vonken EJ, van Osch MJ, Bakker CJ, et al. Measurement of cerebral perfusion with dual-echo multi-slice quantitative dynamic susceptibility contrast MRI. J Magn Reson Imaging. 1999; 10:109–117. [PubMed: 10441012]
13. Miyati T, Banno T, Mase M, et al. Dual dynamic contrast-enhanced MR imaging. J Magn Reson Imaging. 1997; 7:230–235. [PubMed: 9039621]
14. Uematsu H, Maeda M, Sadato N, et al. Blood volume of gliomas determined by double-echo dynamic perfusion-weighted MR imaging: a preliminary study. AJNR Am J Neuroradiol. 2001; 22:1915–1919. [PubMed: 11733325]
15. Vonken EP, van Osch MJ, Bakker CJ, et al. Simultaneous quantitative cerebral perfusion and Gd-DTPA extravasation measurement with dual-echo dynamic susceptibility contrast MRI. Magn Reson Med. 2000; 43:820–827. [PubMed: 10861876]
16. Quarles CC, Gore JC, Xu L, et al. Comparison of dual-echo DSC-MRI- and DCE-MRI-derived contrast agent kinetic parameters. Magn Reson Imaging. 2012; 30:944–953. [PubMed: 22617148]
17. Skinner JT, Robison RK, Elder CP, et al. Evaluation of a multiple spin- and gradient-echo (SAGE) EPI acquisition with SENSE acceleration: Applications for perfusion imaging in and outside the brain. Magn Reson Imaging. 2014 Early View.
18. Tofts PS. Modeling tracer kinetics in dynamic Gd-DTPA MR imaging. J Magn Reson Imaging. 1997; 7:91–101. [PubMed: 9039598]
19. Tofts PS, Brix G, Buckley DL, et al. Estimating kinetic parameters from dynamic contrast-enhanced T(1)-weighted MRI of a diffusable tracer: standardized quantities and symbols. J Magn Reson Imaging. 1999; 10:223–232. [PubMed: 10508281]
20. Schmiedeskamp H, Andre JB, Straka M, et al. Simultaneous perfusion and permeability measurements using combined spin- and gradient-echo MRI. Journal of cerebral blood flow and metabolism : official journal of the International Society of Cerebral Blood Flow and Metabolism. 2013; 33:732–743.

21. Zhang N, Zhang L, Qiu B, et al. Correlation of volume transfer coefficient Ktrans with histopathologic grades of gliomas. J Magn Reson Imaging. 2012; 36:355–363. [PubMed: 22581762]
22. Cha S, Yang L, Johnson G, et al. Comparison of microvascular permeability measurements, K(trans), determined with conventional steady-state T1-weighted and first-pass T2*-weighted MR imaging methods in gliomas and meningiomas. AJNR Am J Neuroradiol. 2006; 27:409–417. [PubMed: 16484420]
23. Ah-See ML, Makris A, Taylor NJ, et al. Early changes in functional dynamic magnetic resonance imaging predict for pathologic response to neoadjuvant chemotherapy in primary breast cancer. Clin Cancer Res. 2008; 14:6580–6589. [PubMed: 18927299]
24. George ML, Dzik-Jurasz AS, Padhani AR, et al. Non-invasive methods of assessing angiogenesis and their value in predicting response to treatment in colorectal cancer. The British journal of surgery. 2001; 88:1628–1636. [PubMed: 11736977]
25. Armitage PA, Schwindack C, Bastin ME, et al. Quantitative assessment of intracranial tumor response to dexamethasone using diffusion, perfusion and permeability magnetic resonance imaging. Magn Reson Imaging. 2007; 25:303–310. [PubMed: 17371718]
26. Batchelor TT, Sorensen AG, di Tomaso E, et al. AZD2171, a pan-VEGF receptor tyrosine kinase inhibitor, normalizes tumor vasculature and alleviates edema in glioblastoma patients. Cancer cell. 2007; 11:83–95. [PubMed: 17222792]
27. Toh CH, Wei KC, Chang CN, et al. Differentiation of primary central nervous system lymphomas and glioblastomas: comparisons of diagnostic performance of dynamic susceptibility contrast-enhanced perfusion MR imaging without and with contrast-leakage correction. AJNR Am J Neuroradiol. 2013; 34:1145–1149. [PubMed: 23348763]
28. Provenzale JM, Wang GR, Brenner T, et al. Comparison of permeability in high-grade and low-grade brain tumors using dynamic susceptibility contrast MR imaging. AJR American journal of roentgenology. 2002; 178:711–716. [PubMed: 11856703]
29. Donahue KM, Krouwer HG, Rand SD, et al. Utility of simultaneously acquired gradient-echo and spin-echo cerebral blood volume and morphology maps in brain tumor patients. Magn Reson Med. 2000; 43:845–853. [PubMed: 10861879]
30. Bonekamp D, Deike K, Wiestler B, et al. Association of overall survival in patients with newly diagnosed glioblastoma with contrast-enhanced perfusion MRI: Comparison of intraindividually matched T - and T -based bolus techniques. J Magn Reson Imaging. 2014
31. Schmiedeskamp H, Straka M, Newbould RD, et al. Combined spin- and gradient-echo perfusion-weighted imaging. Magn Reson Med. 2012; 68:30–40. [PubMed: 22114040]
32. Carroll TJ, Rowley HA, Haughton VM. Automatic calculation of the arterial input function for cerebral perfusion imaging with MR imaging. Radiology. 2003; 227:593–600. [PubMed: 12663823]
33. Newton, AT.; Skinner, JT.; Quarles, CC. Proc Int Soc Magn Reson Med. Salt Lake City, Utah: 2013. Automatic AIF Estimation in Multi-Echo DSC-MRI of Pediatric Patieints: Avoiding the Noise Floor.
34. Liu HL, Pu Y, Liu Y, et al. Cerebral blood flow measurement by dynamic contrast MRI using singular value decomposition with an adaptive threshold. Magn Reson Med. 1999; 42:167–172. [PubMed: 10398963]
35. Kuperman VY, Karczmar GS, Blomley MJ, et al. Differentiating between T1 and T2* changes caused by gadopentetate dimeglumine in the kidney by using a double-echo dynamic MR imaging sequence. J Magn Reson Imaging. 1996; 6:764–768. [PubMed: 8890014]
36. Landis CS, Li X, Telang FW, et al. Determination of the MRI contrast agent concentration time course in vivo following bolus injection: effect of equilibrium transcytolemmal water exchange. Magn Reson Med. 2000; 44:563–574. [PubMed: 11025512]
37. Skinner JT, Yankeelov TE, Peterson TE, et al. Comparison of dynamic contrast-enhanced MRI and quantitative SPECT in a rat glioma model. Contrast media & molecular imaging. 2012; 7:494–500. [PubMed: 22991315]

38. Mills SJ, Patankar TA, Haroon HA, et al. Do cerebral blood volume and contrast transfer coefficient predict prognosis in human glioma? AJNR Am J Neuroradiol. 2006; 27:853–858. [PubMed: 16611778]

39. Liu, Y.; Ding, W.; Bensheng, Q. Proc Int Soc Magn Reson Med. Milan, Italy: 2014. Extravascular extracellular space fraction measurement by DSC-MRI: a theoretical study.

40. Semmineh NB, Xu J, Boxerman JL, et al. An efficient computational approach to characterize DSC-MRI signals arising from three-dimensional heterogeneous tissue structures. PloS one. 2014; 9:e84764. [PubMed: 24416281]

41. Semmineh NB, Xu J, Skinner JT, et al. Assessing tumor cytoarchitecture using multiecho DSC-MRI derived measures of the transverse relaxivity at tracer equilibrium (TRATE). Magn Reson Med. 2014 Epub ahead of print.

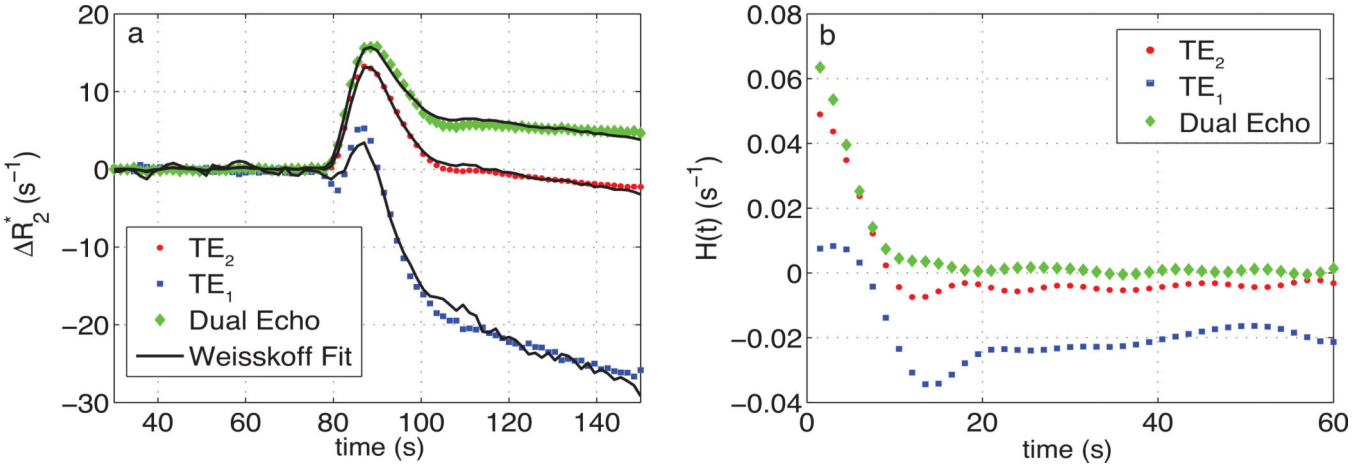

Fig. 1.

a) Representative uncorrected tumor ΔR_2^* time-course and the associated Weisskoff model fit (solid) used to compute K_2 at TE_1 (square), TE_2 (dot), and DE (diamond). b) Corresponding tissue residue function used to compute K_a at TE_1, TE_2, and DE.

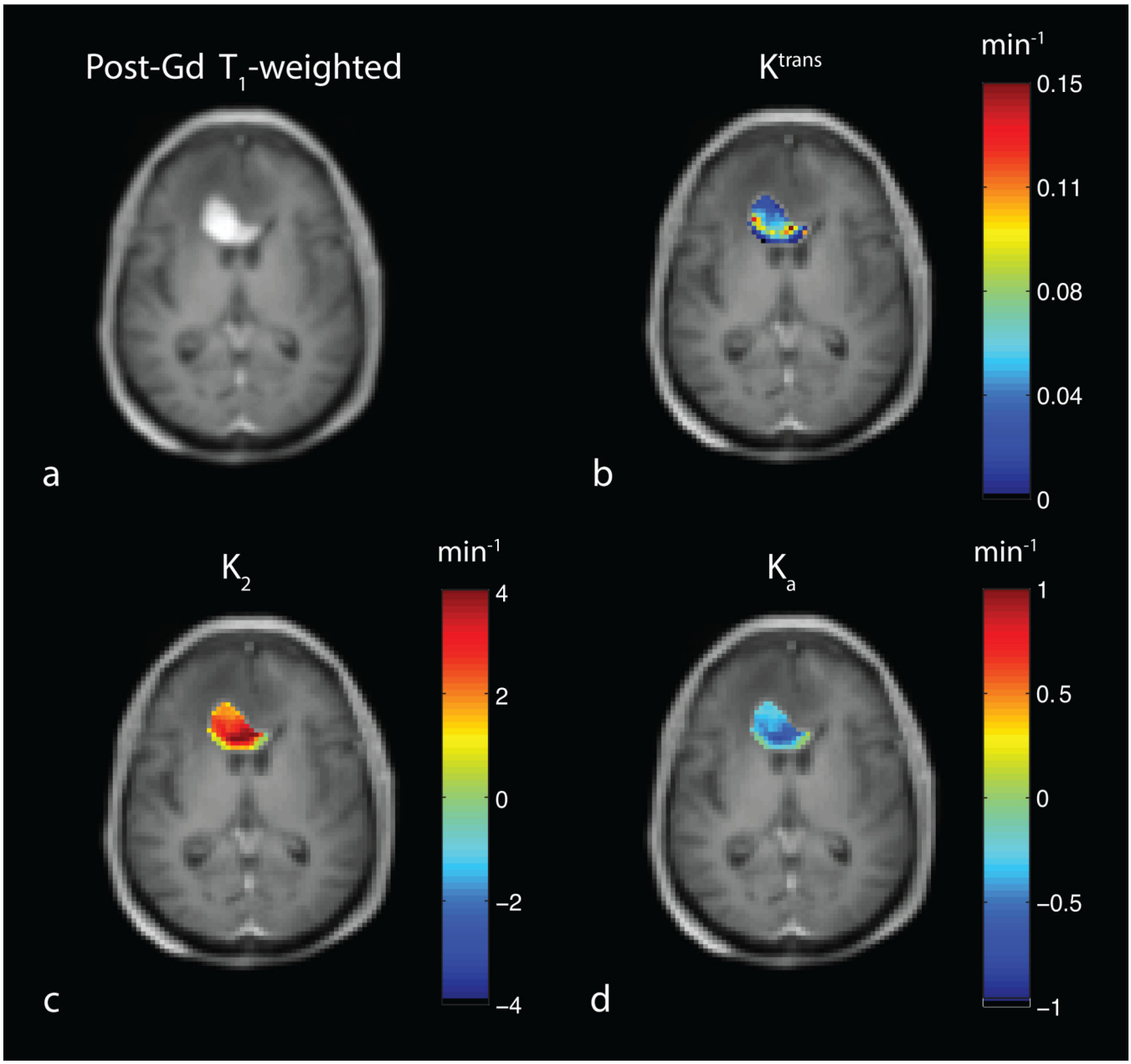

Fig. 2.

a) T_1-weighted post-Gd anatomical image showing a high-grade brain tumor. Example computed permeability maps (units in min^{-1}) for b) K^{trans}, c) K_2 and d) K_a.

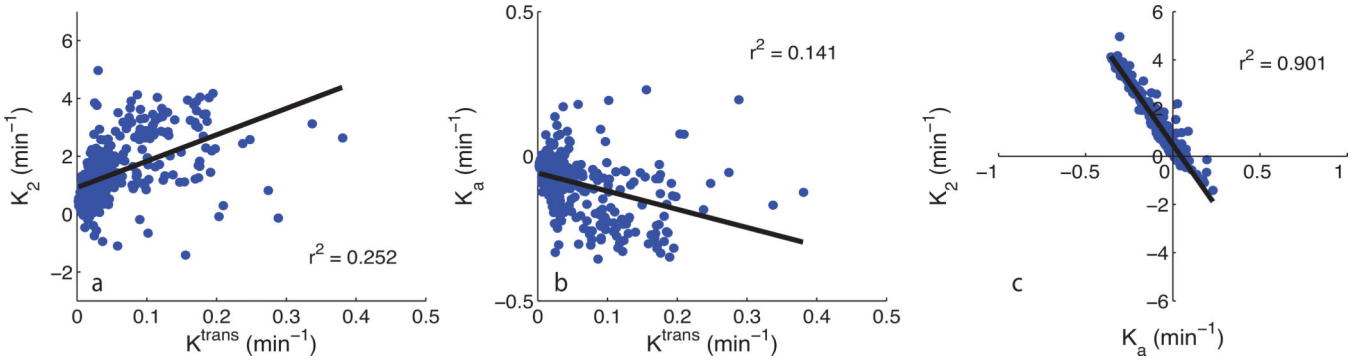

Fig. 3.

a) Example voxel-wise comparison between K_2 at TE_2 and K^{trans}. b) Example voxel-wise comparison between K_a at TE_2 and K^{trans}. c) Voxel-wise comparison between K_2 (y-axis) and K_a (x-axis). Linear regression line shown in black.

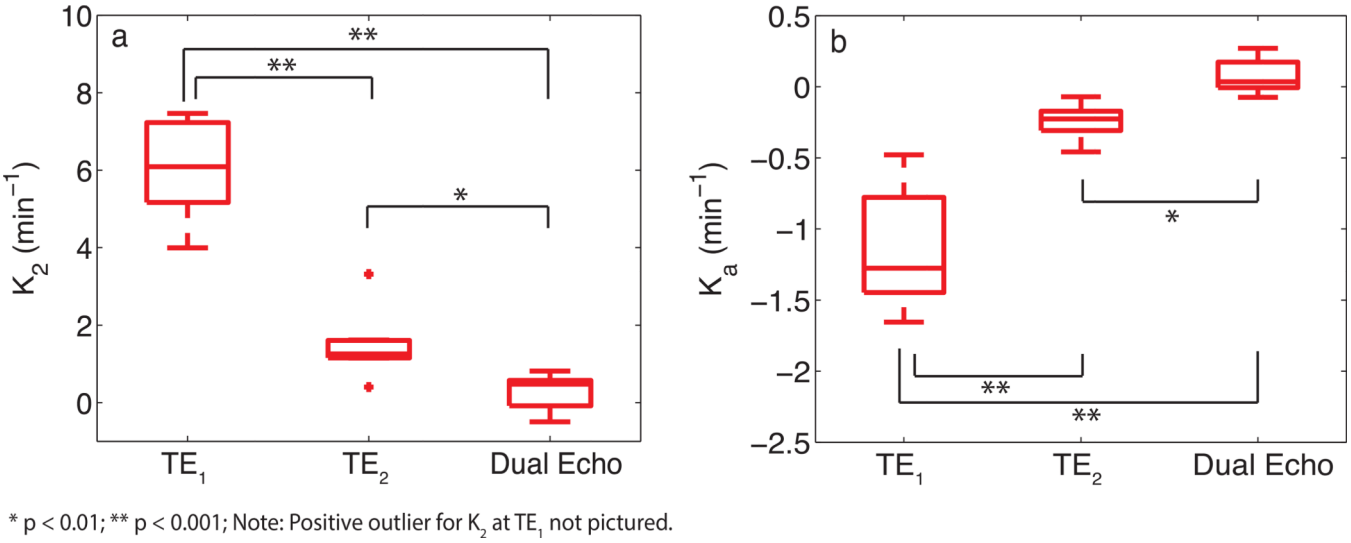

Fig. 4.

Box plots of median parameter estimates (from all patients) calculated at various echo times for K_2 (a) and K_a (b). Box plots display the median, 25th and 75th percentiles (edges of box), and extreme data points (whiskers). Outliers are plotted individually (+). Significance determined by Mann-Whitney U test.

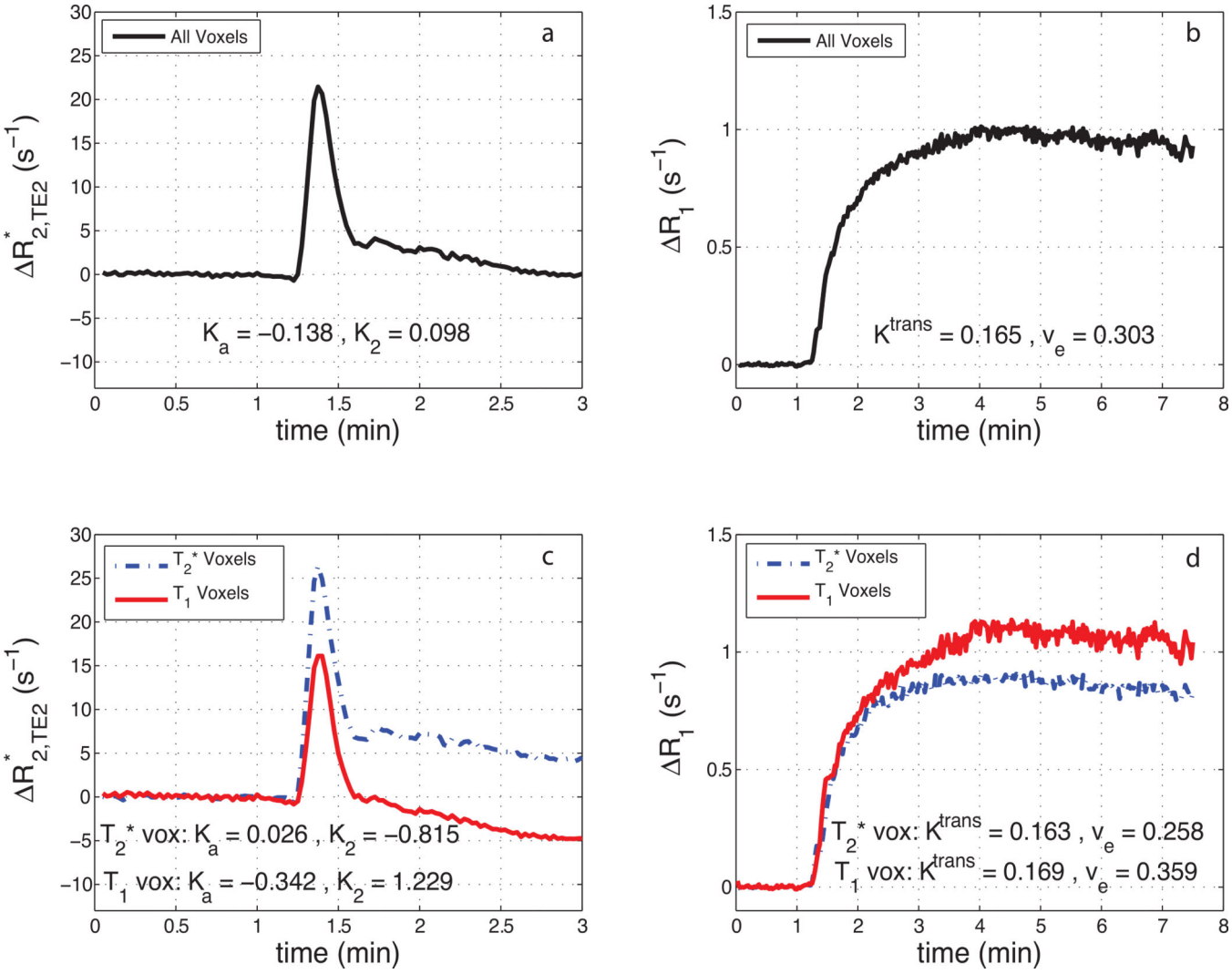

Fig. 5.

a) Example mean ΔR_2^* time-course (TE = 31ms) for a tumor ROI and b) the resulting ΔR_1 time-course. c) Mean ΔR_2^* and d) ΔR_1 time-courses from the same tumor with voxels separated by whether they predominately exhibit T_2^* leakage effects ('T_2^* voxels') or T_1 leakage effects ('T_1 voxels').

Table 1

Patient Demographics

Patient	Age (yr)	Sex	Prior Resection	Pathology	OS (mo)
1	61	Female	Yes	Grade IV Glioblastoma	17.9
2	66	Male	Yes	Grade IV Glioblastoma	18.2
3	65	Male	Yes	Grade III Anaplastic Astrocytoma	N/A
4	51	Male	Yes	Grade IV Glioblastoma	4.3
5	55	Male	No	Grade III Oligodendroglioma	13.1
6	40	Male	Yes	Grade IV Glioblastoma	11.0
7	42	Female	Yes	Grade IV Glioblastoma	N/A

OS = overall survival after radiologically confirmed tumor recurrence/progression

AJNR Am J Neuroradiol. Author manuscript; available in PMC 2016 July 01.

Table 2

Patient specific estimates of DSC-MRI and DCE-MRI parameters separated by the predominant leakage effect

	# Voxels (%)		K_2 (min^{-1})		K_a (min^{-1})		K^{trans} (min^{-1})		v_e	
Patient	T_1	T_2^*	T_1	T_2^*	T_1	T_2^*	T_1	T_2^*	T_1	T_2^*
1	44 (79%)	12 (21%)	1.807	1.205	−0.373	−0.250	0.223	0.066	0.221	0.072
2	214 (45%)	265 (55%)	1.229	−0.815	−0.342	0.026	0.169	0.163	0.359	0.258
3	126 (61%)	79 (39%)	2.374	0.822	−0.372	−0.117	0.089	0.038	0.328	0.150
4	368 (47%)	417 (53%)	1.767	0.700	−0.536	−0.469	0.104	0.078	0.228	0.140
5	187 (56%)	147 (44%)	1.975	0.787	−0.149	−0.025	0.069	0.044	0.284	0.107
6	734 (93%)	52 (7%)	3.726	0.240	−0.256	0.004	0.099	0.050	0.290	0.138
7	16 (64%)	9 (36%)	2.591	0.025	−0.418	0.024	0.200	0.179	0.203	0.107
$mean_w$			2.627	0.289	−0.329	−0.208	0.109	0.092	0.285	0.167

AJNR Am J Neuroradiol. Author manuscript; available in PMC 2016 July 01.